

Near real-time automatic oil spill detection in SAR images**

O.D. Trier^{a,*} and R.B. Huseby^a

^a Norwegian Computing Center, Gaustadalléen 23, P.O. Box 114 Blindern, NO-0314 Oslo, Norway – (trier, huseby)@nr.no.

Abstract – This paper reports on new improvements of an operational oil slick detection algorithm. The existing algorithm is based on a combination of statistical classification and decision rules. We have experimented with using wind information estimated from the SAR scene to compute confidence values.

The wind-based confidence values have some merit, but sometimes they fail. In order to provide reliable confidence values, the estimated wind values can not be used alone.

Another issue is whether monitoring should be performed uniformly over large areas, or if the effort should be concentrated on selected areas. We have analyzed oil spill statistics and generated an oil spill intensity map. This map may be used to focus the oil spill monitoring service. However, some degree of full coverage monitoring should still be performed.

Keywords: Oil pollution, monitoring of ships, confidence estimation, wind, oil spill statistics.

1. INTRODUCTION

Pollution by oil spills in open sea and coastal waters is a major problem due to frequent transport of goods by ships. Many ships dump oil illegally when they think nobody’s watching. Monitoring of oil spills from ships is therefore a high priority task.

Detection of oil spills in SAR amplitude images has been done quite successfully for some time both by manual inspection and automatic detection algorithms (e.g., see the review by Brekke and Solberg, 2005). When the wind is moderate and relatively constant over the entire scene, the oil spills are relatively easy to detect as dark spots due to lower surface roughness than surrounding water. However, in varying wind conditions, low wind areas may appear as dark as the oil spill areas, and can, depending on their shape, be confused with oil spills. Further, local ocean currents may create areas that appear equally dark.

2. EXISTING OIL SPILL DETECTION ALGORITHM

The oil spill detection algorithm can be summarized as follows (Solberg *et al.*, 2007). The details are described further below.

1. Preprocessing and calibration. This includes landmasking the images based on a shoreline database (Wessel and Smith, 1996), followed by range-dependent scaling and conversion to radar brightness values (beta naught values).
2. Dark spot detection.
3. Dark spot feature extraction.
4. Dark spot classification. Each spot is classified as either oil slick or lookalike.

2.1 Dark spot detection

Dark spots are found by dynamic thresholding in multiple resolutions. Different versions of the dark spot detection algorithm have been developed for each sensor. For Envisat ASAR, two resolutions are used, and for Radarsat, three. In a lower resolution image, each pixel is formed by averaging 2×2 pixels in the next higher resolution. Dynamic thresholding is done on each resolution, and combined using the OR operator. Dark spots smaller than 20 pixels are discarded.

The dynamic thresholding is done as follows.

1. For each pixel i , compute the mean value μ and the power-to-mean value σ/μ in a local window of size W , where σ is the standard deviation.
2. Find the homogeneity category k from the power-to-mean ratio in Table 1.
3. Get threshold value $\theta(k)$, in decibels, from Table 1 given the homogeneity category k .
4. Set $T_i = \mu - \theta(k)$.
5. Threshold pixel i with the computed value of T_i .

Table 1. Parameter values for dynamic thresholding.

power-to-mean ratio	Homogeneity category (k)	Thresholds $\theta(k)$, in dB	
		Envisat	Radarsat
> 0.15	1	4,0	4,0
0.05 - 0.15	2	2,7	3,0
0.04 - 0.05	3	2,4	2,0
0.03 - 0.04	4	1,5	1,8
0.015 - 0.03	5	1,3	1,5
< 0.015	6	1,0	1,0

The threshold is thus set adaptively based on estimates of the roughness of the surrounding sea. The motivation for this is as follows. In low wind with many look-alikes, the power-to-mean ratio will be high, and a high contrast between slicks and their surroundings can be expected. As the wind increases, the power-to-mean value will decrease, and the expected contrast between the oil and the surrounding sea will also decrease.

2.2 Dark spot feature extraction

For all the segmented dark spots, features describing shape, contrast, slick surroundings and slick homogeneity are computed.

1. Shape features:
 - a. **Slick complexity**, defined by $C = P^2/A$, where P is the perimeter, and A is area of the region.
 - b. **Slick width**, the ratio between the area of the region and the width of the branches of the skeleton of the region.
 - c. **Slick area**, the size (in number of pixels) of the region.

* Corresponding author.

** This work has been supported by the Norwegian Space Centre.

- d. **First Hu moment invariant**, $\phi_1 = \eta_{20} + \eta_{02}$, for the details see Maitra (1979).
 - e. **Second Hu moment invariant**, $\phi_2 = (\eta_{20} - \eta_{02})^2 + \eta_{11}^2$.
2. Contrast features:
 - a. **Slick local contrast**, the difference between the mean value of the slick and the mean value of a larger window surrounding the slick.
 - b. **Border gradient**, the mean of the magnitude of gradient values of the region border area. The Sobel operator is used to compute the gradient.
 - c. **Smoothness contrast**, $(N_r/G_r)/(N_b/G_b)$ is defined as the ratio between the number of region pixels N_r and the sum of the region pixel gradient values G_r and the ratio of the number of background pixels N_b and the sum of the background gradient values G_b .
 3. Homogeneity features:
 - a. **Surrounding power-to-mean ratio**, computed as σ/μ in a large window containing slick surroundings.
 - b. **Slick power-to-mean ratio**, computed as σ/μ for the slick pixels.
 4. Slick surroundings:
 - a. **Number of detected spots** in the scene.
 - b. **Number of neighboring spots in a large window** centered at the region.
 - c. **Number of neighboring spots in a small window** centered at the region.
 - d. **Distance to closest ship/rig**.
 - e. **Direction of main axis relative to average main axis direction** of surrounding dark spots.
 - f. **Distance to ship/rig along direction** of main axis

Features 1e, 4e and 4f are new, and not mentioned in (Solberg *et al.*, 2007).

2.3 Dark spot classification

In designing a classifier to discriminate between oil spills and look-alikes, several important factors are considered. One factor is the expected number of oil spills compared to the expected number of look-alikes. The number of look-alikes depends on the wind speed and location. With the given segmentation approach, we sometimes observe several hundreds of look-alikes in a single scene during low-wind conditions. In high wind, only a few look-alikes are expected. The expected number of oil spills does not depend strongly on wind speed. In low wind, even very thin oil films are visible in the SAR image, whereas in high wind, only thicker oil films are visible. The expected number of oil spills in a scene might also depend on the location. Oil spills are commonly seen near oil rigs or major shipping lanes. In Section 4 below, statistical analysis is used to produce an intensity map of oil spill incidents.

The classification runs in two steps. First, a statistical classifier is used on a subset of the features. In low wind conditions, this classifier returns a high number of lookalikes as detected oil spills, resulting in a high false alarm rate. In order to reduce this, a number of rules have been developed to eliminate most of the look-alikes.

The result of the automatic classification is a list of possible oil slicks, which are then verified by a skilled operator. A pilot installation is currently being evaluated at Kongsberg Satellite Services (KSAT), Tromsø, Norway.

3. CONFIDENCE ESTIMATION BASED ON WIND SPEED

3.1 Material and methods

Kongsberg Satellite Services (KSAT) have provided 36 Envisat ASAR scenes from 12 December 2007 to 20 May 2008, all containing candidate oil slicks that have been found by their operational oil spill detection service. (Figure 1)

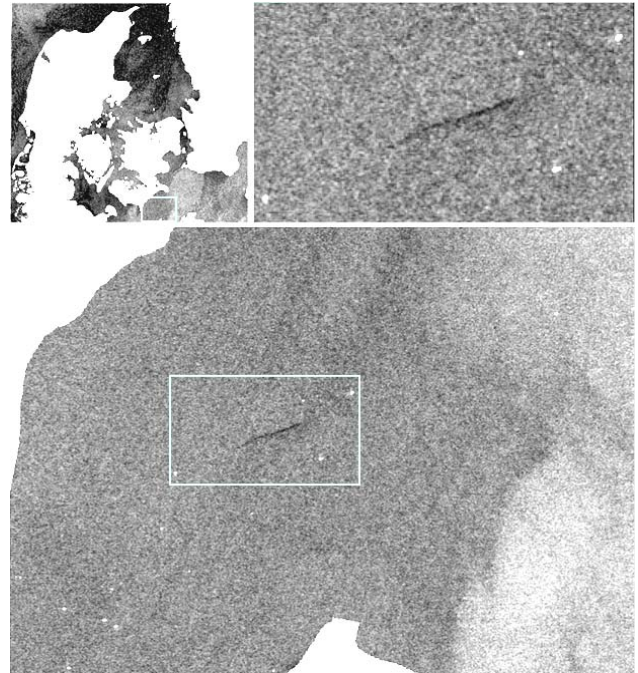


Figure 1. One candidate oil slick in the SAR scene from 12 December 2007. The bright nearby spots may be ships.

In the operational system, for each oil slick candidate, confidence values 'low', 'medium' or 'high' were assigned manually by operators. A fairly long list of criteria was used by the operators when assigning the confidence values. Still, some inter-operator variations have been observed.

In the event that no oil slicks were present in a scene, a 'clean sea' report was issued, accompanied by a confidence value of 'high' or 'medium'.

We have developed a simple method to compute a confidence map to accompany the 'clean sea' report. KSAT is currently evaluating this for possible inclusion in their operational service. The confidence map is generated from the wind speed image as follows. For wind speeds below 3 m/s and above 12 m/s, the confidence is low. For wind speeds between 3 m/s and 7 m/s, the confidence is medium, and between 7 m/s and 12 m/s, high. By applying this rule on a wind speed image (Figure 2), a confidence map is obtained (Figure 3).



Figure 2. Wind speed estimated from SAR image of 12 December 2007. Black = land mask or missing data, gray level intensity is proportional to wind speed.

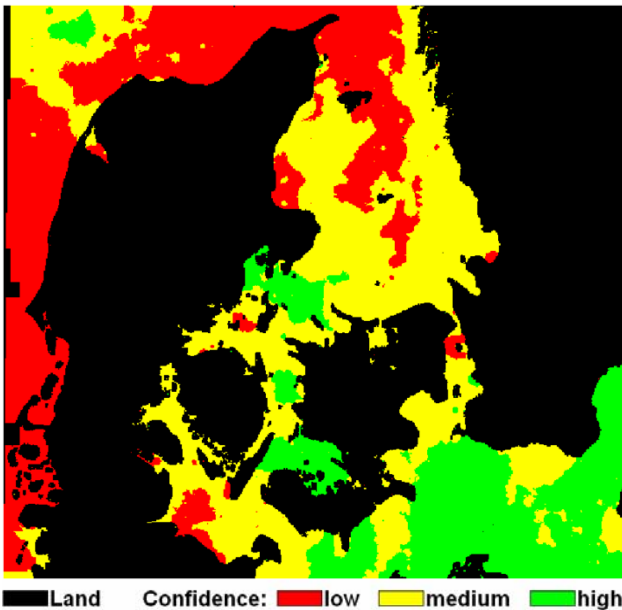


Figure 3. Confidence of 'clean sea' based on wind speed estimated from SAR image. Black means land mask or missing data.

We wanted to study to what extent such confidence maps (Figure 3) could be used to assign confidence values to possible oil slicks (Figure 1).

3.2 Results

Color confidence maps were made for all 36 Envisat ASAR scenes and compared with a manual classification done by the authors (Table 2).

Table 2. Confidence values computed from estimated wind speed versus manual classification.

wind-based confidence	manual classification by the authors	
	lookalike	possible oil slick
low	81	19
medium	26	25
high	1	7

Of the 159 oil slick candidates that the system had detected, we regarded 51 as 'possible oil slicks', which we would like the system to recognize, and the remaining 108 as 'lookalikes'. Of the look-alikes, the system assigned a low confidence value to 75% of them, and medium confidence to 24%. However, for the possible oil slicks, only 13% were assigned a high confidence level. 49% were assigned medium confidence, and 37% low.

3.3 Discussion and conclusions

The confidence image indicates how well the candidate slick stands out from the surrounding sea. However, other factors are also used when manually verifying a candidate oil slick. The presence of nearby ships, especially if one of the ships is located in the direct continuation of an elongated slick, is a clear indication of a true oil slick and the potential polluter. In the close-up section of Figure 1, a ship appears at the lower left corner, in the direct continuation of the candidate slick, making this slick a very probable oil slick. The wind based confidence is, however, medium (Figure 3).

The experiments demonstrate that the wind based confidence values have some merit, but sometimes they fail. In order to provide reliable automatic confidence values, the estimated wind values can not be used alone. In the operational system at KSAT, a fairly long list of criteria is used to manually assign confidence values to each detected slick, and wind speed is regarded as one of the most important criteria.

In order to develop reliable automatic confidence estimation, each criterion should be analysed individually, as we have done with wind speed. Also, combinations of the best individual criteria should be analysed. We plan to do so in a future study.

4. STATISTICAL ANALYSIS OF OIL SPILL DATA

4.1 Material and methods

Kongsberg Satellite Services (KSAT) has through the Marcoast project provided a dataset consisting of 5066 oil slick candidates from 4022 SAR scenes from their operational oil spill detection service to EMSA (European Marine Safety Agency) and other clients (Figure 4). The SAR scenes are from an 18 months period. Since the number of SAR scenes for a given location varies greatly across the study area (Figure 5), a plot of the detections (Figure 4) will give a biased impression of the oil spill frequency. To estimate the real frequency, a coverage frequency distribution may be used. The estimated oil spill frequency f at any location (x,y) , is computed as

$$f(x,y) = \frac{c(x,y)}{s(x,y) \cdot a} \quad (1)$$

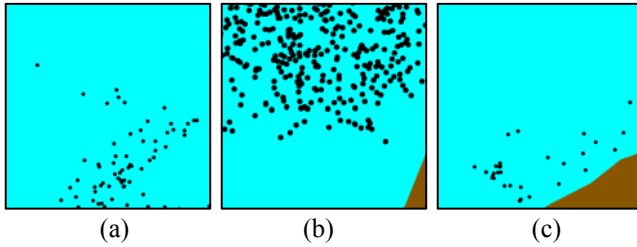


Figure 4. Detected oil slick candidates in an 18 months period, for three small portions of the dataset. Each black dot is an oil spill, cyan is sea and brown is land. (a) a $500 \times 500 \text{ km}^2$ subimage, (b) a $350 \times 350 \text{ km}^2$ subimage, and (c) another $500 \times 500 \text{ km}^2$ subimage.

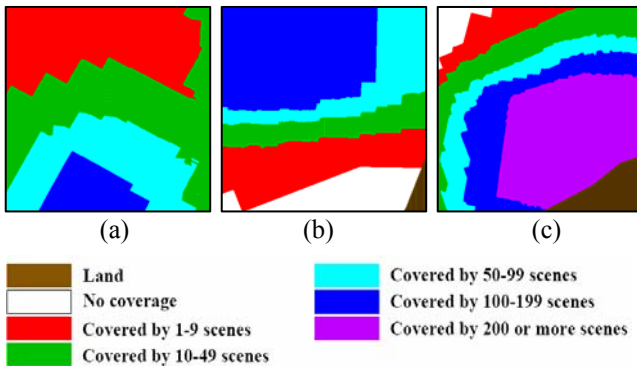


Figure 5. The SAR scene coverage for the same subimages as in Figure 4.

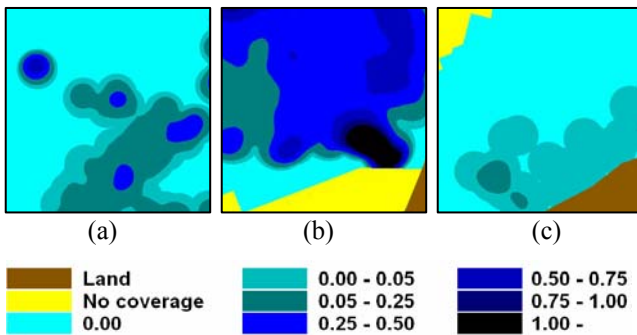


Figure 6. Intensity map for the same subimages as in Figure 4 – Figure 5.

where $c(x, y)$ is the number of candidate slicks in a small neighborhood centered on the location (x, y) , $s(x, y)$ is the number

of SAR scenes covering the location (x, y) , and a is the area of the neighborhood.

4.2 Results

By using Equation 1 on the dataset, an intensity map was produced (Figure 6). As one would expect, locations with many individual slick candidates were marked with high intensity. However, some areas with only a few individual detected oil slicks were also assigned a high intensity, due to the low number of SAR scenes for those locations. For example, there is a single detection in the upper left portion of Figure 4a, but due to the low number of SAR scenes, the intensity is high. Conversely, a moderately high number of detected slicks in Figure 4c resulted in a fairly low intensity (Figure 6c) due to the high number of SAR scenes (Figure 5c). A very high number of detections in the upper half of Figure 4b resulted in a large area with relatively high intensities (Figure 6b), but the highest intensity is found in the lower right quarter of the subimage, in an area with low SAR scene coverage (Figure 5b).

4.3 Discussion and conclusions

The intensity map may be used to focus the oil slick monitoring efforts on high intensity waters. However, one should bear in mind that the areas with a low number of SAR scene coverage also have a relatively large uncertainty in the estimated intensity. A mix of intense monitoring of selected areas combined with a full coverage monitoring may be the best approach.

ACKNOWLEDGEMENTS

We thank Kongsberg Satellite Services for a fruitful collaboration in the project and for providing datasets and the European Marine Safety Agency for permission to use their data.

REFERENCES

- Brekke, C. and Solberg, A. H. S., 2005. Review: oil spill detection by satellite remote sensing. *Remote Sensing of Environment* 95 (1); 1–13.
- Maitra, S., 1979. Moment invariants. *Proceedings of the IEEE*, 67(4); 697-699.
- Solberg, A. H. S., Brekke, C., and Husøy, P. O., 2007. Oil spill detection in Radarsat and Envisat SAR images. *IEEE Transactions on Geoscience and Remote Sensing* 45 (3); 746–755.
- Wessel, P., and Smith, W. H. F., 1996. A global self-consistent, hierarchical, high-resolution shoreline database. *J. Geophys. Res.* 101 (1); 8741–8743.